Astronomy & Astrophysics manuscript no. output
August 26, 2022

Uncertainties in asteroseismic grid-based estimates of halo star ages

S. Moser[1], G. Valle[1], M. Dell'Omodarme[1], S. Degl'Innocenti[1,2], P.G. Prada Moroni[1,2]

[1] Dipartimento di Fisica "Enrico Fermi", Università di Pisa, Largo Pontecorvo 3, I-56127, Pisa, Italy
[2] INFN, Sezione di Pisa, Largo Pontecorvo 3, I-56127, Pisa, Italy

Received ; accepted

ABSTRACT

Context. Stellar age determinations for field stars are crucial to study the Galaxy evolutionary history. So far, the vast majority of researches in literature have been focused on stars with typical disk characteristics.
Aims. The availability of high quality asteroseismic data for stars with typical Halo characteristics makes nowadays possible to extend these investigation. The aim of this paper is to study the precision and theoretical biases in Halo stellar age determination adopting both asteroseismic and classic observational constraints.
Methods. We adopt the well tested SCEPtER pipeline, covering evolutionary phases up to the red giant branch (RGB). The fitting grids contains stars with mass in the range [0.7; 1.0] $M_{\odot}$ and metallicity [Fe/H] from -2.5 to -0.5, typical of the halo population. We investigate several scenarios, characterised by different adopted observational uncertainties. We also assess the impact of systematic discrepancies between the recovery grid models and target stars by computing several synthetic grids of stellar models with perturbed input physics.
Results. Asteroseismic age estimates are more precise for old metal-poor stars as compared to more metallic stars. In our reference scenario (errors in $\Delta\nu$ and $\nu_{\rm max}$ of 2.5% and 5% respectively) stars in main sequence (MS) or sub-giant branch (SGB) were recovered with a typical 10/20% precision, while the precision in RGB stars was about 60%. However recent observations allow tighter constraints in asteroseismic parameters by about a factor of 3. With this assumption the age precision in RGB improved to 20%, while little modifications occur in the other analysed evolutionary phases. The investigation on the relevance of systematic discrepancies between grid models and target stars showed that a mismatch in the mixing-length parameter value between grid and targets (from 1.9 to 1.74) led to significant biases in MS (about 10%) and smaller ones in SGB and RGB. The neglect of microscopic diffusion effect in the recovery grid led to a typical 40% bias in MS.
Finally, we applied the age estimation technique to stars in globular clusters, adopting typical observational uncertainties from the literature. We found a precision in age estimates around 20% for MS stars and up to 40% for RGB stars. These uncertainties are worse than the ones obtained with classical methods, which are therefore still to be preferred. We also applied the SCEPtER pipeline to the age determination of M4, relying on asteroseismic data for seven RGB stars from literature. We obtained a cluster age $11.5^{+1.7}_{-3.8}$ Gyr and mass at the TO $0.86^{+0.10}_{-0.03}$ $M_{\odot}$, in good agreement with literature results.

Key words. Asteroseismology – methods: statistical – stars: evolution – stars: oscillations – stars: low-mass – stars: fundamental parameters

1. Introduction

An accurate knowledge of the stellar ages is fundamental to recover the evolutionary history of the Galaxy. However age estimation of field stars is notoriously a difficult problem due to several uncertainties both in the stellar models used to date stars and in the observations (see Soderblom 2010, for a review). As a consequence, the precision of age determinations obtained from the comparison between theory and observation for classical observables is generally poor, with errors larger than 40% in several cases (e.g. Jørgensen & Lindegren 2005; Takeda et al. 2007; Soderblom 2010; Sanders & Das 2018). The problem is even more severe for old, distant stars in the Galactic halo, making the exploration of early Galactic history problematic (see e.g. Jofré & Weiss 2011; Guo et al. 2016; Das et al. 2020; Matsuno et al. 2021).

The recent development of precision asteroseismology, thanks to the satellite missions, such as CoRoT (Appourchaux et al. 2008; Michel et al. 2008; Baglin et al. 2009), *Kepler* (Borucki et al. 2010; Gilliland et al. 2010) and TESS (Ricker et al. 2015), has led to a noticeable improvement of stellar age estimations. Several analyses in the literature (e.g. Gai et al. 2011; Chaplin et al. 2014; Casagrande et al. 2014; Valle et al. 2015c) have shown that it is possible to achieve a 10/20% average precision in estimated ages, depending on the evolutionary phase of the target star.

The vast majority of researches have been focused on stars near the Sun with typical disk characteristics, simply because the bulk of asteroseismic data are available for such targets. Only recently, asteroseismic investigations of halo star ages have been performed (e.g. Montalbán et al. 2021; Matsuno et al. 2021; Grunblatt et al. 2021).

The aim of the present paper is to evaluate the typical uncertainties and biases in the age determination of field stars with characteristics typical of the Halo of the Milky Way. The analysis presented hereafter is conducted assuming the availability of both global asteroseismic quantities (i.e. the average large frequency spacing and the frequency of maximum oscilla-

Send offprint requests to: G. Valle, valle@df.unipi.it

tion power) and classical observables (effective temperature and [Fe/H]). The work addresses both the theoretical assessment of expected errors and the exploration of possible bias sources – due to uncertainty in the stellar models input physics – and includes applications to real data. We closely follow the methodology presented in Valle et al. (2015c), where a similar analysis has been performed for stars with higher metallicities and for a wide age range. This allows a direct comparison of the results, thus highlighting the differences in age estimation caused by the difference in the explored metallicity range. Finally, we compare the precision of the asteroseismic age determinations against those from the isochrone fitting method for the nearby globular cluster (GC) M4 that is, the only GC for which asteroseismic data are available.

The paper is organized as follows. In Sect. 2 we discuss the method and the grids adopted in the estimation process. Sect. 3 and 4 contain the results and the bias sources investigation. Sect. 5 addresses the M4 fit. Some concluding remarks can be found in Sect. 6.

2. Grid-based recovery technique

2.1. Estimation method

We adopted the SCEPtER scheme[1] extensively described in Valle et al. (2014). For reader's convenience we summarize the basic aspects of the procedure. We let $\mathcal{S}$ be a star for which the following vector of observed quantities is available: $q^{\mathcal{S}} \equiv \{T_{\rm eff,\mathcal{S}}, [{\rm Fe/H}]_{\mathcal{S}}, \Delta\nu_{\mathcal{S}}, \nu_{\rm max,\mathcal{S}}\}$. Then we let $\sigma = \{\sigma(T_{\rm eff,\mathcal{S}}), \sigma([{\rm Fe/H}]_{\mathcal{S}}), \sigma(\Delta\nu_{\mathcal{S}}), \sigma(\nu_{\rm max,\mathcal{S}})\}$ be the nominal uncertainty in the observed quantities. For each point j on the estimation grid of stellar models, we define $q^j \equiv \{T_{{\rm eff},j}, [{\rm Fe/H}]_j, \Delta\nu_j, \nu_{{\rm max},j}\}$. We let $\mathcal{L}_j$ be the likelihood function defined as

$$\mathcal{L}_j = \left(\prod_{i=1}^{4} \frac{1}{\sqrt{2\pi}\sigma_i}\right) \times \exp\left(-\frac{d_j^2}{2}\right) \quad (1)$$

where

$$d_j = \left\| \frac{q^{\mathcal{S}} - \tilde{q}^j}{\sigma} \right\| \quad (2)$$

The likelihood function is evaluated for each grid point within 3σ of all the variables from $\mathcal{S}$. We let $\mathcal{L}_{\rm max}$ be the maximum value obtained in this step. The estimated stellar mass, radius, and age are obtained by averaging the corresponding quantity of all the models with likelihood greater than $0.95 \times \mathcal{L}_{\rm max}$.

The technique can also be employed to construct a Monte Carlo confidence interval for stellar parameters. To this purpose a synthetic sample of $n = 10\,000$ stars is generated, following a multivariate normal distribution with vector of mean $q^{\mathcal{S}}$ and covariance matrix $\Sigma = {\rm diag}(\sigma)$. The medians of the n objects stellar parameters are taken as the best estimate of the true values, and the 16th and 84th quantiles are adopted as a 1σ confidence interval.

2.2. Standard stellar models grid

The standard estimation grid of stellar models was computed using FRANEC stellar evolution code (Degl'Innocenti et al. 2008), in the same configuration that was adopted to compute the Pisa Stellar Evolution Data Base[2] for low-mass stars (Dell'Omodarme et al. 2012; Dell'Omodarme & Valle 2013).

The resulting grid consisted of 572 880 points (880 points for 651 evolutionary tracks), corresponding to evolutionary stages from the ZAMS to the helium flash. Models were computed for masses in the range [0.70; 1.00] $M_\odot$ with a step of 0.01 $M_\odot$. This mass range was chosen to include the halo population of the Milky Way which shows ages generally older than 10 Gyr; it is thus expected that stars above $\sim 1\ M_\odot$ have already gone past the red giant branch (RGB) and so they are not in evolutionary phases of interest for this work. The upper limit of 1.0 $M_\odot$ was imposed to mitigate the impact of the edge effects, that will be discussed later. Stars with $M < 0.7\ M_\odot$, that are likely to be still in the main sequence (MS), were not included due to lack of asteroseismic observations in this mass range. The initial metallicity [Fe/H] was assumed in the range $[-2.5; -0.5]$, with a step of 0.1 dex, to include the bulk of halo stars. We did not theoretically investigate the effects of uncertainties in α enhancement, and we assumed a solar-scaled heavy-element mixture by Asplund et al. (2009) for both grid models and synthetic observations. This assumption was dropped when estimating the age of the GC M4 in Sect. 5, were we assumed an α enhancement of 0.4 (Marino et al. 2008). The initial helium abundance was obtained using the generally adopted linear relation for the helium to metal enrichment ratio $Y = Y_p + \frac{\Delta Y}{\Delta Z} Z$ with a primordial ^{4}He abundance value $Y_p = 0.2471$ from Planck Collaboration et al. (2020), and $\Delta Y/\Delta Z = 2.03$ (Tognelli et al. 2021). The models were computed following the mixing length formalism for convective envelopes assuming a mixing-length parameter $\alpha_{\rm ml} = 1.90$, as obtained from a calibration on the M4 photometric data, in particular in the RGB region (see Fig. 5). Atomic diffusion was included adopting the coefficients given by Thoul et al. (1994) for gravitational settling and thermal diffusion. To prevent the surface helium and metal depletion for stars without a convective envelope, a diffusion inhibition mechanism similar to the one discussed in Chaboyer et al. (2001) is adopted. For the outermost 1% in mass of the star, the diffusion velocities were multiplied by a suppression parabolic factor that takes value 1 at the 99% in mass of the structure and 0 at the base of the atmosphere. Further details about the input physics adopted in the computations are available in Valle et al. (2014, 2009).

The average large frequency spacing $\Delta\nu$ and the frequency of maximum oscillation power $\nu_{\rm max}$ were obtained using a simple scaling from the solar values (Ulrich 1986; Brown et al. 1991; Kjeldsen & Bedding 1995):

$$\frac{\Delta\nu}{\Delta\nu_\odot} = \sqrt{\frac{M/M_\odot}{(R/R_\odot)^3}}\ , \quad (3)$$

$$\frac{\nu_{\rm max}}{\nu_{\rm max,\odot}} = \frac{M/M_\odot}{(R/R_\odot)^2 \sqrt{T_{\rm eff}/T_{\rm eff,\odot}}}. \quad (4)$$

The validity of these scaling relations in the RGB phase has been questioned in recent years (e.g. Epstein et al. 2014; Gaulme et al. 2016; Viani et al. 2017) and using them to fit real observational RGB stars can lead to systematic biases. Corrections to these scaling relations have been investigated by many authors in different ranges of mass, metallicity and evolutionary phases (e.g. White et al. 2011; Sharma et al. 2016). In Rodrigues et al. (2017) theoretical models were used to determine corrections to the reference values $\Delta\nu_{\rm ref}$ to be used instead of the solar large

[1] An R library providing the estimation code and grid is available at CRAN: http://CRAN.R-project.org/package=SCEPtER.

[2] http://astro.df.unipi.it/stellar-models/

frequency separation, $\Delta\nu_\odot$, as a function of mass, metallicity and ν_{max}. They showed that for RGB stars, with metallicity inside the range $-0.75 \leq$ [Fe/H] ≤ -1.00, mass range $0.8 \leq M_\odot \leq 1.0$ and ν_{max} range $10 \leq \nu_{max} \leq 40$ μHz, the correction at the $\Delta\nu_{ref}$ value to be applied is about -5%. **This result is confirmed by the analysis by Tailo et al. (2022) for RGB stars in M4, who obtain a correction from -3% in the initial part of RGB to -5% for stars in near the RGB bump.** We adopted this correction in Sect. 5, when estimating stellar parameters for stars in M4[3]. The reliability of scaling relation is instead of minor relevance when testing the internal grid accuracy and biases, because we used exactly the same scaling relations to compute $\Delta\nu$ and ν_{max} in both the artificial stars and the models. Therefore no correction was applied in these cases.

3. Age estimates

The age recovery procedure was first tested on a synthetic dataset obtained by sampling $N = 30\,000$ artificial stars from the same standard estimation grid of stellar models used in the recovery procedure itself. For each synthetic object a Gaussian noise was added to the observable quantities, to simulate the effects of typical uncertainties on the observations. In this work we were interested in stars with characteristics typical of the Milky Way Halo, so we only sampled stars between 9.5 Gyr and 13.8 Gyr. The lower limit was established from the belief that the vast majority of Halo stars are older than 10 Gyr (Jofré & Weiss 2011), whereas the upper limit comes directly from recent estimations of the Universe's age (Planck Collaboration et al. 2020).

We separately analysed stars in different evolutionary phases: MS, Sub Giant Branch (SGB) and RGB. Stars evolved past the RGB were not considered due to the necessity to include in the calculations the uncertainty of the mass loss efficiency; this would require a much extended model grid significantly increasing the computational times. The synthetic sample contains an equal number of models from each analysed evolutionary phase. To obtain a more realistic population, stars were sampled adopting a typical initial mass function distribution filter (e.g. Salpeter 1955; Kroupa 2002). Due to the selection restrictions, the synthetic sample does not cover the whole mass range of the estimation grid, because stars older than 10 Gyr and more massive than $\sim 1.0\ M_\odot$ have already evolved past the RGB phase. For the same reason, the mass range of interest differs for each investigated evolutionary phase.

The aims of this analysis are multifold:

a) a direct comparison with the results in Valle et al. (2015c) obtained in a different metallicity range (hereafter Case 1, C1);
b) a realistic estimate of the uncertainties in asteroseismic field Halo star ages (C2);
c) an estimate of the uncertainty in the asteroseismic derived age for GC stars (C3).

Therefore the sketched analysis was repeated assuming different sets of observational uncertainties in both classical and asteroseismic parameters.

More in detail, the observational errors adopted for the C1 case were identical to those in Valle et al. (2015c), which presented the same analysis for a population typical of the Milky Way's disk, i.e. 2.5% in $\Delta\nu$, 5% in ν_{max}, 100 K in T_{eff}, and 0.1 dex in [Fe/H]. The adoption of the same set of observational errors allowed us to best disentangle possible differences and trends due to the differences in the stellar metallicity range between the two investigations. **Moreover these uncertainties are close to that reported by Stello et al. (2022) for TESS analysis of RGB stars (i.e 5% in ν_{max}x and about 3% in $\Delta\nu$), thus providing a useful insight about the uncertainty in age estimates achievable by TESS.**

Table 1. Observational errors adopted in the Monte Carlo experiments for the three investigated scenarios.

Scenario	T_{eff} (K)	[Fe/H] (dex)	$\Delta\nu$	ν_{max}
C1	100	0.10	2.5%	5%
C2	100	0.05	0.6%	1.7%
C3	150	0.03	1%	4%

However, if one is interested in assessing the best precision nowadays achievable for asteroseismic age estimates on Halo stars, these observational errors are overestimated in few cases. Recent works investigated asteroseismic data from the Kepler field (Yu et al. 2018) to study Halo stars (e.g. Montalbán et al. 2021; Matsuno et al. 2021; Grunblatt et al. 2021), reporting a median uncertainty in asteroseismic constraints of 0.6% in $\Delta\nu$ and 1.7% in ν_{max} and typical uncertainties in classical observables of 100 K in T_{eff} and 0.05 dex in [Fe/H]. These are the values adopted in C2.

Stars in GC are an important part of the population of the Halo. Unfortunately, at present, the only GC in which asteroseismic observations of some stars are available is M4. This situation is expected to improve in the future and some space missions have been proposed explicitly to target stars in clusters (e.g. HAYDN, Miglio et al. 2021). Thus it's interesting to compare asteroseismic age estimates for GCs with the ones by the robust classic isochrone fitting method. Due to the relative high stellar density of globular cluster stars and the large distances, observational uncertainties are higher than the mean ones for field stars. In C3 we adopted an uncertainty for the asteroseismic observables of 1% in $\Delta\nu$ and 4% in ν_{max} from Miglio et al. (2016), while for classical data, we assumed an error of 150 K in T_{eff} and 0.03 dex in [Fe/H], typical values found in recent literature. **The error on T_{eff} will be later justified and comes from the adoption of scaling relations on photometric data, similarly to what was done in Malavolta et al. (2014).**

The three investigated scenarios, and their uncertainties, are summarized in Table 1.

3.1. C1: comparison of uncertainties in typical Halo and Disk stars

Adopting the SCEPtER algorithm (Sect. 2.1), we estimated ages of synthetic stars and compared the results to actual values. A positive relative error indicates that the age of the star was overestimated by the recovery procedure. Figure 1 shows the trend of the age relative errors versus the true mass of the star, its relative age – conventionally set to zero at the start of the selected evolutionary phase and defined as the ratio between the current age of the star and its age at the end of the same evolutionary phase – and its metallicity [Fe/H][4]. The figure also shows the relative error envelopes obtained by evaluating the 16th and 84th quantiles (1 σ) and 2.5th and 97.5th quantiles (2 σ) of the age relative

[3] The correction was not applied to the grid, but to the observables to make the procedure faster and easier.

[4] This is the present surface [Fe/H] value, different from the initial one due to microscopic diffusion.

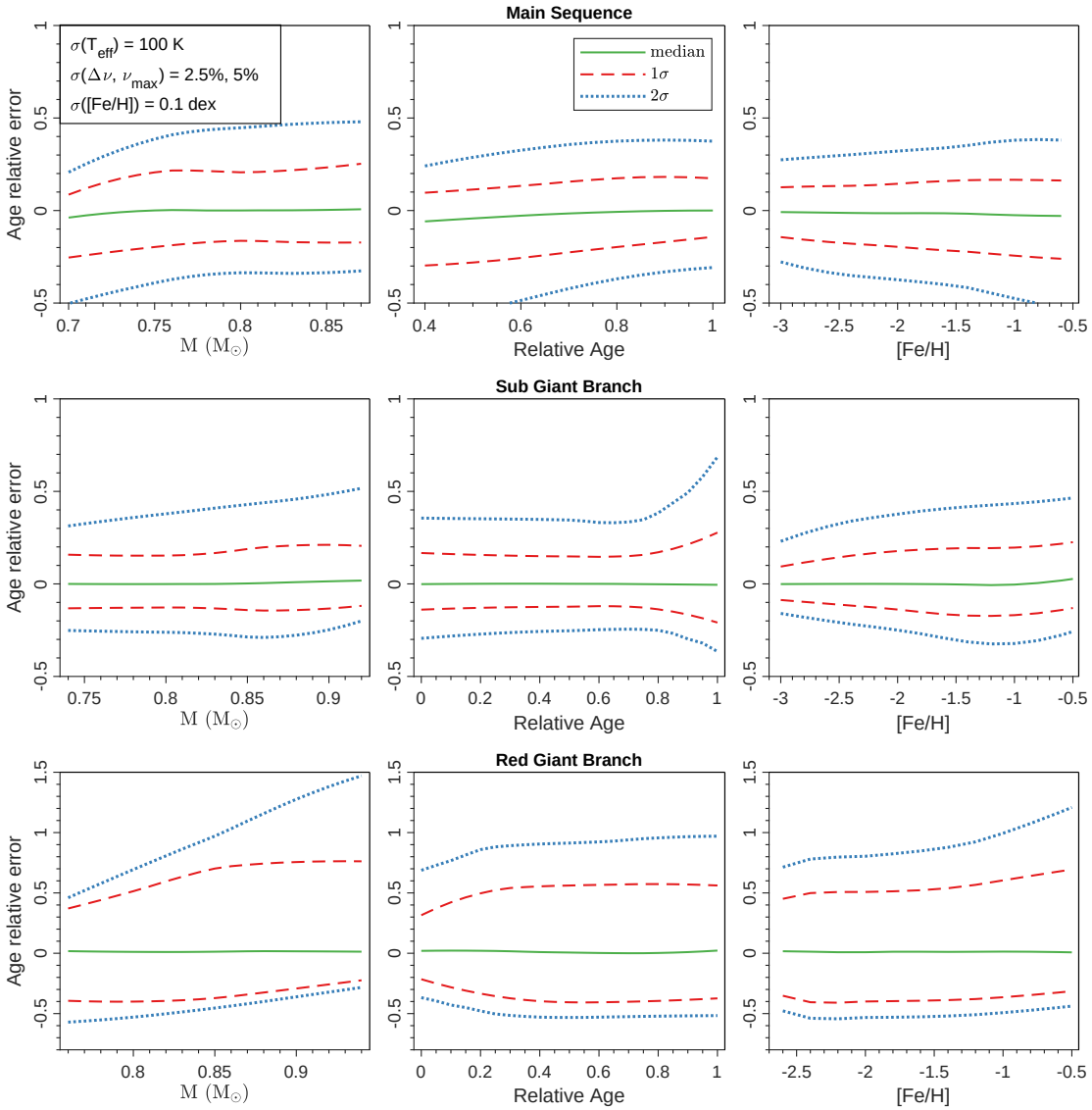

Fig. 1. Age estimate relative errors as a function of the true mass (left panels), relative age (central panels), and metallicity [Fe/H] (right panels) of the star. From top to bottom, the panels show relative age errors for MS, SGB and RGB respectively. The green solid line marks the error medians. The red solid line is the 1σ error envelope, while the blue dashed one marks the position of the 2σ envelope (see text). A positive relative error indicates that the reconstructed age of the star is overestimated with respect to the true one.

error over a moving window[5]. The position of the 1 σ envelope and of the median of the age relative error in dependence on the true mass of the star and on its relative age are reported in Appendix in Tables A.1 to A.6 in the section labelled C1.

The median relative errors are compatible with zero in all analysed cases, meaning that the recovery procedure is not intrinsically biased, as already verified for higher metallicities in Valle et al. (2015c). A −5% departure from zero is seen for MS stars with relative ages lower than 0.5 due to an edge effect. Since the sample age range is fixed, lower relative ages correspond to lower masses that, due to their long MS lifetimes, are still far away from the turn-off. Masses smaller than $M \sim 0.74$ correspond to the grid lower edge, therefore their mass can only be overestimated, and the age underestimated. For this reason the distribution of errors for these lower masses is slightly shifted and the median falls slightly off zero, which could be falsely interpreted as a bias in the age estimation. The edge effect can also be seen in the top-middle and top-left panel of Fig. 1. Edge effects were already pointed out in previous works (e.g. Valle et al. 2014) thus the estimation grid was purposefully generated larger with respect to the values of interest for this work to mitigate this problem. Being the observation of asteroseismic parameters for Halo MS stars with $M < 0.75\ M_{\odot}$ highly improbable in the near future, the mass range of interest is about [0.8; 0.95] $M_{\odot}$.

Apart from the already mentioned edge effect, age relative errors for MS stars are almost constant, between 10% and 20%, as a function of mass and relative age.

Age relative errors slightly increase with metallicity. This effect arises from the grid morphology in the 4D observational parameters space. Lower metallicity models are more spread apart, so given a set of observable uncertainties, it is easier to discriminate the correct solution **(see fig. 2)**. Typical age relative errors obtained in this work are generally smaller than those reported

[5] The half-width of the window is typically 1/12-1/16 of the range spanned by the independent variable. This choice allows us to maintain the mean relative error in the 1 σ envelope owing to Monte Carlo sampling at a level of about 5%, without introducing too much smoothing.

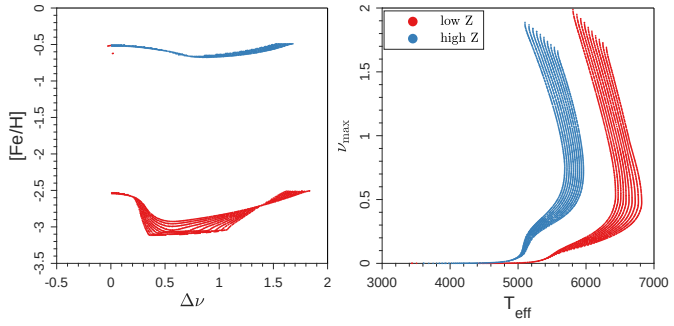

Fig. 2. Distribution of identical stellar models ($M < 0.8\ M_{\odot}$) at high ([Fe/H]= −0.5) and low ([Fe/H]= −2.0) initial metallicity. Low metallicity models occupy a larger region in the observational parameter space.

by Valle et al. (2015c) for stars with chemical compositions typical of the Milky Way's disk, by as much as 10%, possibly due to an intrinsic difference in age estimation precision at different metallicity. This comparison is however not straightforward because the considered stellar population differs in mass range, Valle et al. (2015c) stars being more massive. As pointed out by Valle et al. (2015c) the difference in the age estimation error can be as big as 15% between 0.8 $M_{\odot}$ and 1.4 $M_{\odot}$ stars. Furthermore, Valle et al. (2015c) sample contains young MS stars, for which relative age errors can be larger than 100%.

Age relative errors in SGB do not change with the mass of the star and are generally constant throughout their entire, short lifetime, except for the final part where, as shown the middle-central panel of Fig. 1, the 1σ and 2σ error envelopes slightly increase. During this final part of the SGB, theoretical models converge toward small observational parameters space because they are approaching the RGB, where the distribution of effective temperatures is narrower. The same happens to asteroseismic parameters as they depend on T_{eff}. The packing of theoretical models make the estimation process intrinsically more difficult leading to larger age uncertainties. The results shows again an increase of age errors for higher metallicities, although, in this case there are no previous studies for metallicity ranges to confront with.

The analysis for RGB stars shows an important degradation in age estimation precision, with errors as large as 60%. The main reason is, again, the packing of the models in the observable parameters space. As already reported in the literature, the models in this evolutionary phase have a narrow distribution in effective temperatures that is also much more dependent on the metallicity with respect to MS stars, thus the mass recovery is more difficult leading to a larger age errors (see e.g. Basu et al. 2010; Valle et al. 2015b). Due to these large errors and the fact that negative relative errors cannot be greater then -100%, the resulting age distributions are slightly skewed towards positive errors. Indeed, for more favourable conditions in which age errors are smaller even for the RGB phase, distributions are again symmetric as it can be seen in cases that are discussed later.

3.2. C2: effect of realistic uncertainties in halo field stars

The results of the analysis for C2 are reported in Tables A.1 to A.6 under the section C2 and are also shown in Fig. 3, where 1 σ envelopes are compared with the ones for the C1 and C3 scenarios. During the MS and SGB phases,one sees a reduction of $\sim$ 5% in the 1 σ error envelopes, mainly due to the slightly better precision of $T_{\rm eff}$. The result that effective temperature uncertainty is the main contributor to the age estimation error for MS stars is a confirmation of what was already noticed in Valle et al. (2018a) for stars in the Milky Way's disk. Effective temperature is strongly linked to the mass of the star, thus a better constraint on $T_{\rm eff}$ leads to a better mass estimate, which in turn is highly correlated to the stellar age. During the MS phase, an improvement in asteroseismic data or in metallicity precision does not lead to substantial decrease in the age estimation error. For SGB stars, again, improving the precision in asteroseismic data does not have a significant effect. Improving metallicity precision, however, indeed leads to a significant reduction of the age relative error, except for relative age above 0.8, where models occupy a smaller region in the observational parameters space.

For RGB stars the reduction of the age errors is significant, as big as 20/30%. The smaller age estimation uncertainties lead to symmetric error envelopes, confirming that the asymmetry seen in the standard case was due to large observational errors. The largest contribution to the error reduction is due to the improvement of the asteroseismic data, confirming again the results shown in Valle et al. (2018a) for more metal-rich stars. Reducing the error in effective temperature does not lead to a noticeable effect. The evolutionary tracks of RGB models are very close in effective temperature, therefore an unrealistically small uncertainty in effective temperature would be needed to efficiently improve the recovery of the stellar mass and age. Indeed, with an error of $\sim$ 80 K on $T_{\rm eff}$ a 3 σ confidence interval covers almost the entire range of possible effective temperatures for RGB stars. Finally, the improvement the metallicity estimate has almost no effect on the age recovery precision.

3.3. C3: effect of realistic uncertainties for GC stars

The results for the C3 scenario are shown in Tables A.1 to A.6 in the corresponding sections. Figure 3 shows the 1 σ error envelopes as a function of true mass, relative age and metallicity compared with the results for the standard and field stars cases. In MS and SGB phases the typical error is a bit larger compared to the standard case. This is due to the larger uncertainty on $T_{\rm eff}$, although this error increase is partially counterbalanced by the reduction of the uncertainty of the other observables, especially of the metallicity.

In the RGB phase, however, the slight reduction of the asteroseismic data error leads to a noticeable reduction of the age relative uncertainty. Therefore, for RGB stars in GCs (which are the only ones with available observational data, except for horizontal branch stars, not studied in this work) one expects a typical age uncertainty of about 35/45%.

4. Stellar model uncertainty propagation

When grid-based techniques are applied to real stars rather than to synthetic ones, the accuracy of age estimates depends on the systematic discrepancies between the adopted stellar models and observational data. **The uncertainties of the input physics and physical mechanisms adopted in stellar evolutionary codes leads to indeterminacy in the grid-based results. This issue has been extensively discussed in many works (e.g. Basu et al. 2012; Lebreton et al. 2014; Valle et al. 2014, 2015c), and it is well known that the variability in age estimates obtained by different estimating pipelines is of the same order of the statistical uncertainty on the age as obtained by a single pipeline (Basu et al. 2012; Valle et al. 2015c; Silva Aguirre et al. 2017; Valle et al. 2020; Tayar et al. 2022). The aim of this section**

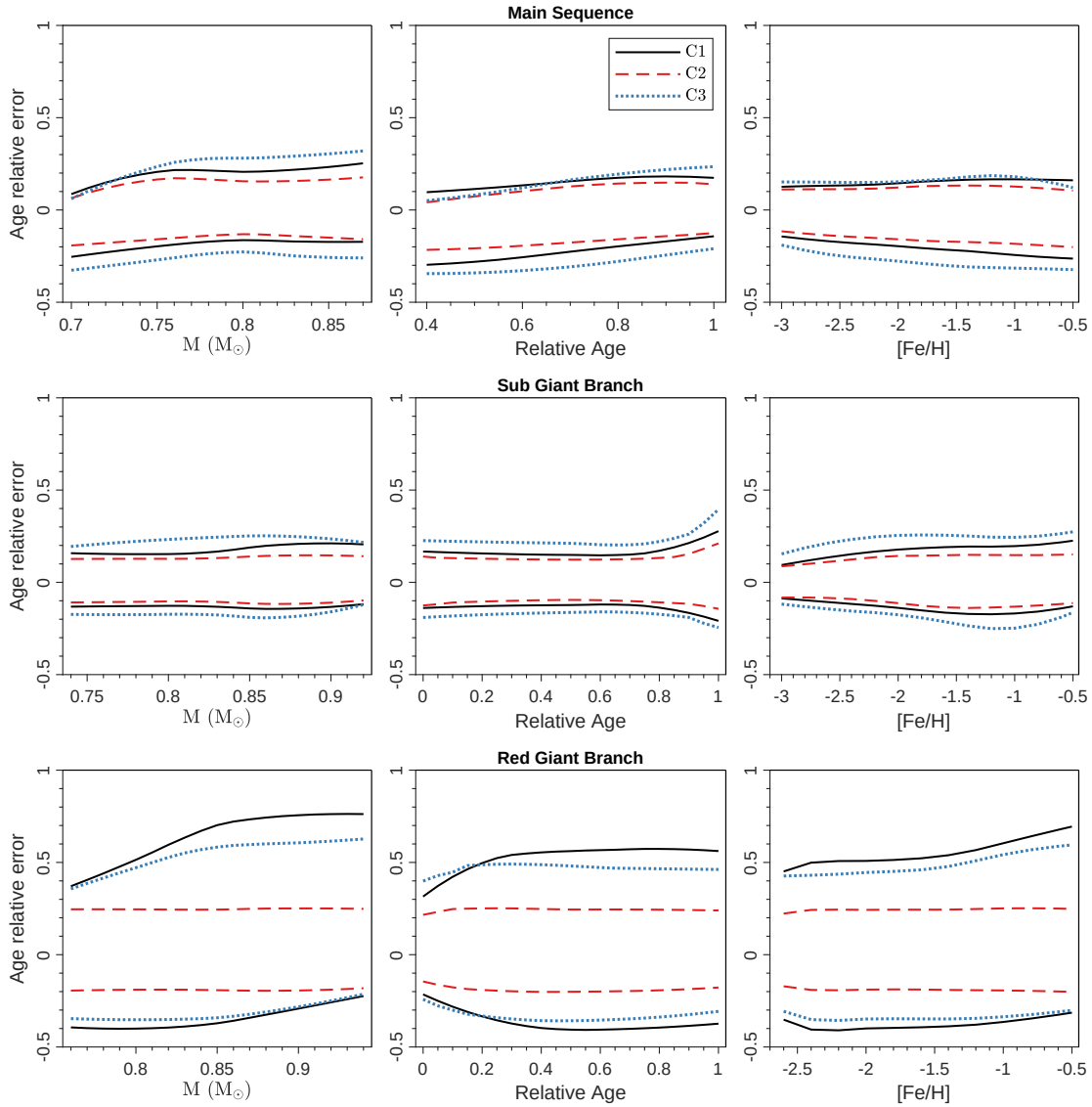

Fig. 3. *Top row*: age estimate relative errors as a function of the true mass (*left panel*), relative age (*central panel*), and metallicity [Fe/H] (*right panel*) for MS star. *Middle row*: same as in the *top row* but for SGB stars. *Bottom row*: same as in the *top row* but for RGB stars. Black lines mark the 1 σ age estimation error envelopes computed adopting C1 uncertainties. The dashed red lines show 1 σ envelopes for the C2 scenario. The blue dotted lines mark 1 σ envelopes for the C3 scenario (see text and Table 1).

is to quantitatively analyze some of the biases occurring due to different modeller choices for age estimates of old, metal poor stars.

We focus our analysis on the uncertainty in the mixing-length parameter and in the efficiency of element diffusion. Contrarily to what has already been done in Valle et al. (2015c), we do not take into account the uncertainty in the original helium abundance. In fact Valle et al. (2015c) showed that the effect of this uncertainty is quite negligible; moreover for low metallicity stars the variations on the initial He abundance due to different $\Delta Y/\Delta Z$ values is not significant.

We performed these estimates following Valle et al. (2014). More in detail, we computed some non-standard grids of perturbed stellar models by individually varying the chosen input to their extreme values, while keeping all the others fixed to their reference values. Artificial stars were then sampled from these grids, and their ages were estimated using the standard one. In both cases, presented in Sect. 4.1 and Sect. 4.2, the assumed uncertainty in the observables is the one of the C2 case: $\sigma(T_{\rm eff})$ = 83 K, $\sigma(\Delta\nu)$ = 0.6%, $\sigma(\nu_{\rm max})$ = 1.7% and σ([Fe/H]) = 0.05 dex.

4.1. Mixing-length value

It is increasingly apparent that the use of a solar-calibrated mixing-length value for stars that differ from the Sun in mass, composition, and/or evolutionary phase could not be appropriate (see e.g. Deheuvels & Michel 2011; Bonaca et al. 2012; Mathur et al. 2012; Tanner et al. 2014; Trampedach & Stein 2011; Magic et al. 2015; Yıldız 2007; Clausen et al. 2009). To quantify the effect of varying the efficiency of the super-adiabatic convective transport, we computed one additional non standard grid of stellar models by assuming the solar calibrated mixing-length parameter $\alpha_{\rm ml}$ = 1.74. Then, we built a synthetic dataset of N = 30 000 artificial stars (for the already discussed evolutionary phases) sampling them from the non-standard grid. The age of the synthetic stars have been then estimated using the standard grid for the recovery, which assumes our M4 calibrated value

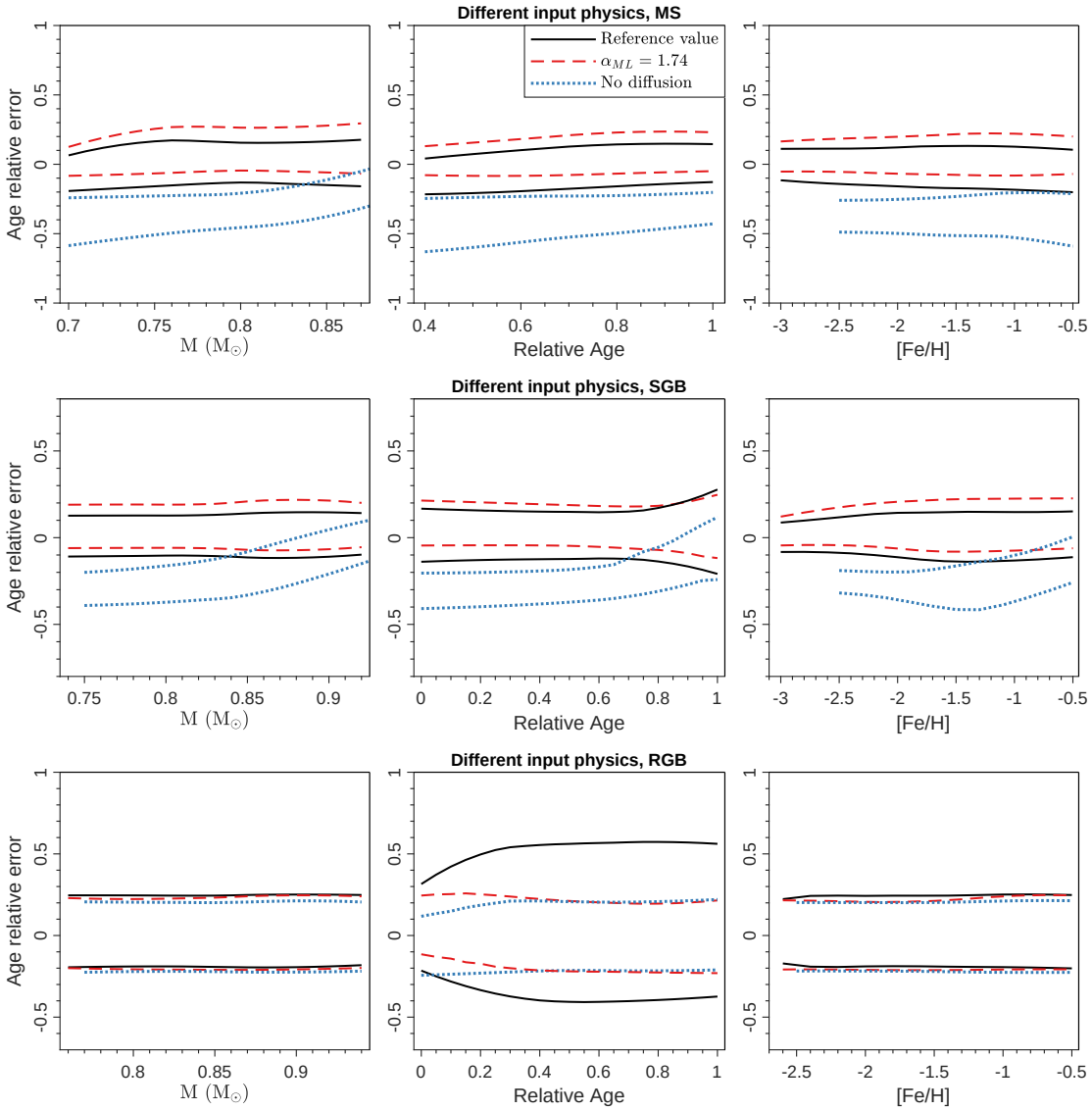

Fig. 4. Envelope of age-estimate relative errors as a function of mass and relative age of the star with different values on the input physics compared to the estimation grid. The black line corresponds to the standard case; the red one to a different efficiency of the external convection; the blue one to stars without diffusion whose age is estimated by adopting a grid of models with diffusion.

$\alpha_{\rm ml}$ = 1.90. The results of these tests are presented in section "$\alpha_{\rm ml}$ = 1.74" in all the tables.

The bias for MS stars is noticeable, with a departure of the median from zero of about 10%, meaning that in general old stars in the halo can be overestimated in age by as much as 1 Gyr, if the efficiency of convection is not well parameterized. Artificial stars with varied $\alpha_{\rm ml}$ occupy a different location in the 4D space of the observable quantities with respect to standard models of the same mass and age. In particular, models with a less efficient convection (smaller $\alpha_{\rm ml}$) are colder than their corresponding model with $\alpha_{\rm ml}$ = 1.90). **Besides this direct effect, which is the main responsible of the age bias (see the analysis in Valle et al. 2018a)**, the mixing length value modification also has an effect on the asteroseismic data, which depend on $T_{\rm eff}$ through the scaling relations of Eqs. (3) and (4). This difference in the observable parameters leads the algorithm to wrongly select stars smaller masses that, due to the longer evolutionary times, are usually older, thus explaining the positive age bias.

During the SGB phase the distance in the parameters space among evolutionary models with different mixing-length efficiency is reduced compared to the MS case, however the effect is still present, resulting in a smaller but still present bias that is no bigger than 5%.

In the RGB phase, there is a trend inversion. At the start of the RGB the bias is still small and positive in accordance to what can be seen at the end of the SGB phase. However, for increasing values of relative age, the bias reduces, until it reaches zero at around 30% of the RGB lifetime. Then, the bias in age estimation is inverted and for more evolved RGB models, the algorithm wrongly select models with a higher mass, thus generally younger stars, leading to a small negative bias that does not exceed 4%.

This trend is caused by the progressive clumping of the grid in the observational parameters space, that becomes more severe as the evolution in the RGB proceeds. In particular, during the RGB evolution, the difference in effective temperature among models of different mass drastically reduces. This effect coupled with the relatively large uncertainty in $T_{\rm eff}$, leads to the consequence that, contrarily to MS phase, the algorithm cannot use this observable to efficiently recover mass and age. Instead,

the stellar age recovery is mainly based on the asteroseismic parameters, as discussed in Valle et al. (2018a). It is possible to show that at fixed mass, metallicity and evolutionary phase the asteroseismic parameters are smaller for a lower efficiency of the convection. This means that the algorithm is lead to choose a more massive model, thus causing the negative age bias. The fundamental role of the effective temperature was checked by a direct computation, repeating the age estimation without the effective temperature observational constraint. In this case the age bias in the MS reversed, becoming negative, thus confirming the dominant impact of $T_{\rm eff}$ in this phase. Ultimately, this result is another supporting evidence to the fact that grid based estimates and their biases are extremely dependent on the adopted observational constraints and on the studied evolutionary phases (see e.g Basu et al. 2012; Valle et al. 2015a).

In conclusion, it is interesting to notice that the bias for low metallicity stars is generally lower than the one for typical disk stars, evaluated in Valle et al. (2015c) (the comparison stands only for MS stars as the other two evolutionary phases were not studied). This trend in metallicity is also visible at the top-right panel of Fig. 4. **This is likely a result of the grid being more compact for less metallic stars as already discussed. This leads to models with different convection efficiency to be more close in the parameter space, in particular in the asteroseismic parameters, thus biases result to be smaller.**

4.2. Element diffusion

Valle et al. (2014) discussed the importance of considering the effects of the microscopic diffusion when determining stellar parameters by means of grid-based techniques, assessing the bias in mass and radius estimates when element diffusion is neglected. While microscopic diffusion has been proved to be efficient in the Sun (see e.g. Bahcall et al. 2001), with a related 15% uncertainty, its efficiency in Galactic GC stars is still debated (see e.g. Gruyters et al. 2014; Nordlander et al. 2012; Gratton et al. 2011; Korn et al. 2007).

To conservatively estimate the age bias which could be due to microscopic diffusion effects, we sampled stars from a non-standard grid with models computed without diffusion, and then we recovered their age through the standard grid, where diffusion is taken into account. Results are shown in Fig. 4 and tabulated in the sections labelled "no diffusion" in all the tables for different evolutionary phases. As already seen in previous works (Valle et al. 2014, 2015c), biases can be quite large in MS with values around 40%.The effects increases with the decrease of the stellar mass, due to the larger MS evolutionary times which allows a stronger diffusion effect on the models. This large bias arises from both the evolutionary time change and the surface temperature and chemical composition variation, due to diffusion. In general, the recovered is biased toward higher masses, leading to large negative biases for the estimated ages.

However totally neglecting diffusion is probably a too crude assumption; in this way we conservatively obtained an upper bound for the possible age bias. A realistic bias, due to microscopic diffusion uncertainty, would be smaller, even though still important.

A small bias persists during the major part of the SGB evolution, at least until the first dredge-up undoes the most of diffusion effects on the chemical composition. Finally, during the RGB phase these biases are quite negligible, due to the completion of the first dredge-up and to the RGB evolutionary timescale, which is much faster than the diffusion timescale. As discussed above, a more realistic case would lead to even smaller biases.

5. Asteroseismic and classical age of the globular cluster M4

In this section the asteroseismic age estimation technique is applied to some stars of the M4 globular cluster, the only one for which asteroseismic parameters are available in the literature. The estimated mean age is then compared to the one obtained adopting the classical isochrone fitting method. The analysis is similar to that presented by Miglio et al. (2016). Miglio et al. (2016) made available global asteroseismic parameters from the K2 mission campaign which detected clear solar-like oscillations for seven RGB stars and one star in the red part of the horizontal branch (HB).

The present analysis includes the seven RGB stars only. The HB star investigation is avoided because this evolutionary phase is not included in our models grid; moreover the position of stars inside the HB region depends on the stochastic mass loss during the RGB phase, so modeling HB stars would introduce other systematic uncertainty sources.

For the analysis we adopted the average metallicity of the cluster available in the literature, i.e. [Fe/H] = -1.17 ± 0.03 (Bailin 2019). Effective temperatures adopted in Miglio et al. (2016) came from Marino et al. (2008), derived from spectroscopic data. However, a direct comparison showed that these values do not agree well with the theoretical isochrone that better fits the color magnitude diagram of the cluster, a problem evident also in the paper by Miglio et al. (2016). Therefore we derived new values for the effective temperature, adopting a widely used metallicity dependent relation between the stellar colour and its temperature

$$\theta = b_0 + b_1 C + b_2 C^2 + b_3 [\mathrm{Fe/H}] + b_4 [\mathrm{Fe/H}]^2 + b_5 [\mathrm{Fe/H}] C, \quad (5)$$

where $T_{\rm eff} = 5040/\theta$ and C is the colour of the star in a given photometric system.

We used seven colours for each star: four colours from the Stetson et al. (2019) catalogue (classical photometric bands from the Johnson-Cousins filter system) and three colours from the third early data release of Gaia Riello et al. (2020). Coefficients b_i for the Johnson-Cousins colours can be found tabulated in Ramírez & Meléndez (2005), while the more recent coefficients for the Gaia colours were obtained from Mucciarelli & Bellazzini (2020). For each star, the temperatures derived from the seven colours were averaged to compute a single estimate of the effective temperature, while errors were computed through error propagation rules using uncertainties given in the respective works. **No correction due to differential reddening was adopted, as our results are very close to the ones presented in Malavolta et al. (2014) where such correction was indeed done.** Table 2 summarises the data; it can be seen that our estimates of effective temperatures are generally 100 K higher than those in Marino et al. (2008), however they are in good agreement with the values from Malavolta et al. (2014), obtained from photometric data too (although their dataset do not cover the entire sample of stars for which asteroseismic parameters are available). The computed values are in better agreement with extrapolated temperatures from the theoretical isochrone that fitted the cluster CMD.

5.1. Stellar models grid

The estimation grid was again computed using the FRANEC code. The [Fe/H] range was chosen to be [-1.3; -0.9], to comfortably contain the 3 σ confidence interval for the estimated value

Table 2. Physical properties for the seven RGB stars for which Miglio et al. (2016) reported unequivocal solar-like oscillations.

ID	$\Delta\nu$ [μHz]	ν_{max} [μHz]	T_{eff} [K] ± 100 K Miglio et al. (2016)	T_{eff} [K] ± 150 K This work
S1	1.83±0.02	11.1±0.4	4585	4671
S2	2.55±0.04	17.2±0.7	4715	4767
S3	2.62±0.04	17.7±0.7	4710	4815
S4	2.64±0.02	18.5±0.7	4715	4801
S5	4.14±0.02	32.5±1.3	4847	4964
S6	4.30±0.02	32.9±1.3	4842	4976
S7	4.30±0.02	34.3±1.4	4805	4915

Notes. The first column reports the ID used in Miglio et al. (2016) to identify the seven RGB stars. The second, third and fourth columns show the global seismic parameters and the effective temperatures from Miglio et al. (2016). In the last column the effective temperatures computed in this work are shown.

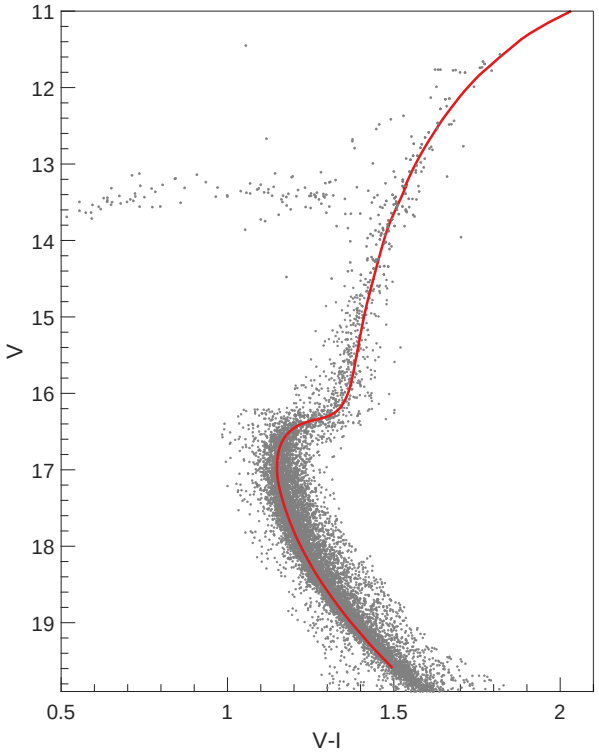

Fig. 5. Theoretical 12 Gyr isochrone red line) superimposed to M4 data from Stetson et al. (2019). The isochrone was computed for [Fe/H] = -1.17 and Y = 0.252. The value of the mixing-length parameter α_{ml} = 1.90 was chosen to best represent the RGB region. The adopted distance modulus and reddening are from Hendricks et al. (2012).

of [Fe/H]=-1.17. The grid includes a total of 16 different metallicities with finer metallicity steps close to the central value. The metallicity, Z, value was derived from iron abundance, assuming an α-enhancement of 0.4 (Marino et al. 2008).

The adopted mass range is [0.76; 1.10] $M_{\odot}$, obtained from a trial and error procedure and it's large enough to keep the mass estimation results far from the edges of the grid, to avoid the previously discussed edge effects. The value of the mixing-length parameter α_{ml} was set to 1.90, because theoretical isochrones computed adopting this value were seen to agree well with the photometric RGB of M4 (see Fig. 5).

Since the evolutionary phase of the stars is known, we kept in the grid only models in the RGB. This implied removing stars with a mass smaller than ~ 0.80 $M_{\odot}$ as they have not yet reached the RGB. From the literature it's known that the M4 turn-off mass is around 0.84 $M_{\odot}$ which, coupled with the already discussed little precision in age and mass estimation for RGB stars, means that results distributions were likely to undergo a small deformation due to edge effects. Further edge effects are introduced because we eliminated from the estimation grid all models older than the Universe, as they would lead to implausible results. Infact from the literature we expect M4 to have an age of about 12 Gyr old and with predicted errors for the asteroseismic method of the order of 40% the estimated age confidence intervals could overcome the present age of the Universe. However, we quantified these edge effects **simply by repeating the computation without cutting the grid and comparing the results**. It was found that central values of age and mass differ by no more than 4% and 1%, respectively, between the two cases, therefore the decision to exclude models with implausible ages appears justified.

Table 3. Mass, radius, and age inferred using SCEPtER for the seven RGB stars observed in M4 from Miglio et al. (2016). For each quantity is reported the central value, (q50) and the 1 σ envelope (q16, q84).

quantile	Mass [$M_{\odot}$]	Radius [$R_{\odot}$]	Age [Gyr]
S1			
q16	0.82	15.94	8.26
q50	0.85	16.18	12.35
q84	0.94	16.79	13.50
S2			
q16	0.82	12.77	7.15
q50	0.86	13.03	11.66
q84	0.98	13.68	13.43
S3			
q16	0.82	12.54	7.50
q50	0.85	12.77	12.08
q84	0.97	13.37	13.45
S4			
q16	0.84	12.60	5.61
q50	0.93	13.06	8.64
q84	1.06	13.62	12.73
S5			
q16	0.83	9.32	6.86
q50	0.89	9.53	10.05
q84	1.00	9.93	12.94
S6			
q16	0.82	9.08	9.73
q50	0.84	9.13	12.69
q84	0.90	9.34	13.35
S7			
q16	0.83	9.09	6.82
q50	0.89	9.30	10.28
q84	1.00	9.68	12.86

5.2. results

Table 3 shows the results of mass, radius and age estimation of the seven stars of M4. As q50 are reported the central values, while q16 and q84 represent the lower and upper 1 σ confidence interval. Due to the fast evolution of stars past the TO, it's possible to assume that the mass of RGB stars is close to the TO mass. Computing the median of all the obtained q50 values it's possible to estimate the TO mass, $M = 0.86^{+0.10}_{-0.03}$ $M_{\odot}$, where uncertainties are derived from the median values of q16 and q84 of each star. This result is in good agreement with the estimate by

Table 4. Age estimates for NGC 6121 found in the literature.

Reference	Age [Gyr]
Caputo et al. (1985)	12±2
Hansen et al. (2002)	12.7±0.7
Salaris & Weiss (2002a)	11.7±1.1
Dotter et al. (2010b)	12.5±0.5
VandenBerg et al. (2013b)	11.5±0.4
Wagner-Kaiser et al. (2017)	$13.493^{+0.007}_{-0.027}$

Miglio et al. (2016) and with the TO mass found from isochrone fitting, which is around 0.85 $M_{\odot}$.

In particular, it can be seen that the lower error in age is around 30%, as reported in Table A.3 and Table A.6, for stars with $M \sim 0.86\ M_{\odot}$ and relative age ~ 0.9 which is where the RGB bump occurs. The median age, which we assume as the estimate of the cluster age, is $11.5^{+1.7}_{-3.8}$ Gyr. This value is in good agreement with results from the literature (e.g. VandenBerg et al. 2013a; Dotter et al. 2010a; Salaris & Weiss 2002b, see Table 4), although errors are very large, as it was expected from the analysis in Sect. 3.3. The upper error, however, has been artificially reduced by removing from the grid all the models older than the Universe. Therefore, we see an upper error of $\sim 10\%$ instead of $\sim 40\%$.

The previous results were obtained after the star labelled S4 in Miglio et al. (2016) was removed from the analysis. In fact, it was deemed to be an outlier, due to its estimated age and mass being significantly different from the other six stars.

In closing the section it worth discussing the fact that the cluster age was obtained without imposing a common age and composition in the fit of single stars. This approach has the merit of a straightforward implementation (e.g. Gai et al. 2011; Sandquist et al. 2016). However, as extensively discussed in Valle et al. (2018b), whenever common age and composition constraints are imposed, the cluster age estimation significantly shrinks towards the common value. This suggests that a different approach to cluster age estimation – e.g. by Markov Chain Monte Carlo (MCMC) methods – can possibly get a precision comparable to classical methods. A detailed computation of the cluster age by this different technique is however outside the scope of the present paper.

6. Conclusions

We performed a theoretical investigation to quantify the uncertainty in the age estimation of field and cluster stars with characteristics typical of the Halo of the Milky Way. To do this we employed the SCEPtER pipeline to estimate the ages of a large sample of synthetic, metal poor, and old stars in MS, SGB and RGB evolutionary phases, to mimic halo filed stars. We used both classical ($T_{\rm eff}$, [Fe/H]) and asteroseismic ($\Delta\nu$, $\nu_{\rm max}$) observables.

We investigated several scenarios, characterised by different adopted observational uncertainties. First, to highlight, in a consistent way, differences in age estimation precision between Halo and Disk population, we adopted the same observational uncertainties used in Valle et al. (2015c) for disk stars. We found that the asteroseismic age estimates are more precise for old metal-poor stars as compared to more metallic stars. This is because the less metallic stars are usually more spread apart in the adopted observational constraints space; this makes it easier the reconstruction the models mass, which is tightly correlated to the age. A large discrepancy in age estimation precision between MS/SGB and RGB stars was detected, with the former being recovered with a typical precision around 10/20% while the latter can be recovered with a much lower precision ($\sim 60\%$). This discrepancy stems again from the morphology of the estimation grid that is much more clumped for RGB stars.

However at present is possible to achieve somewhat smaller uncertainties than the ones adopted in Valle et al. (2015c). Therefore we repeated the analysis by assuming typical uncertainties in the observables from the recent works by Montalbán et al. (2021) and Matsuno et al. (2021). Results show a slightly better precision of age estimation for MS and SGB stars, mainly due to better constraints in effective temperature and metallicity. However, for RGB stars the improvement is relevant: the average expected uncertainty decreases to about 20%. This large error reduction is mainly due to the improvement of the observed asteroseismic parameters.

To analyse the effects of systematic discrepancies between grid models and observed stars we analysed, as already done in Valle et al. (2015c) for disk stars, the effects on age estimation of the still present uncertainties on the convection and microscopic diffusion efficiency. We found that a difference in the mixing-length parameter between synthetic stars and the estimation grid models leads to significant biases in MS, caused by the effective temperature differences. The algorithm is thus led to mistake the mass of the star and consequently its age. This bias is smaller for SGB stars, because models with different $\alpha_{\rm ml}$ are closer to one another in the observational parameter space compared to MS stars. In the RGB phase the bias is opposite. In this evolutionary phase the discriminating power of the effective temperature is much reduced because of the packing of the tracks. In this situation the fit is mainly based on the values of the asteroseismic parameters which lead to prefer more massive, therefore younger, models. This inversion confirms that generalizing grid based results for evolutionary phases or observational constraints different than those directly studied can led to severe mistakes.

Finally, we explored the application of this age estimation technique to stars in GCs, for comparison with the results of the classical isochrone fitting age estimation method. As typical observational uncertainties we adopted the ones obtained by Miglio et al. (2016) for stars in M4, the only GC for which asteroseismic data are available until now. The analysis with synthetic stars show that, as the uncertainties in effective temperature and asteroseismic parameters are quite large, the expected precision of age estimates is around 20% for MS stars and up to 40% for RGB stars. Classical GC age estimation methods such as the vertical method, can obtain significantly better accuracy. A more accurate comparison of the precision achievable by classical and asteroseismic based methods would involve adopting MCMC methods and explicitly imposing a common age in the fit of asteroseismic data. However, this comparison is outside the scope of the present paper.

To empirically explore the impact of systematic discrepancies between model and real data, we applied the asteroseismic age estimation method to seven RGB stars in M4, for which high quality asteroseismic observation are available (Miglio et al. 2016), repeating the procedure already done by (Miglio et al. 2016) and Malavolta et al. (2014). To do this we recomputed the seven stellar effective temperatures, using photometric data from Stetson et al. (2019) and the third early data release of Gaia (Riello et al. 2020). This procedure was necessary because the temperatures from Marino et al. (2008), adopted by (Miglio et al. 2016), did not satisfactory agree with the ones of the isochrone that best fitted the color magnitude diagram of the cluster. Our estimates of effective temperatures are generally 100 K higher

than those in Marino et al. (2008), however they are in good agreement with the values from Malavolta et al. (2014) and are in better agreement with extrapolated temperatures from the theoretical isochrone that fitted the CMD.

We also applied correction to the scaling relations for the asteroseismic parameters as the analysed M4 stars are all in the RGB phase, close to the RGB bump, where these corrections are important. The asteroseismic age and mass at the TO ($11.5^{+1.7}_{-3.8}$ Gyr and $M = 0.86^{+0.10}_{-0.03}\ M_{\odot}$, respectively) are in good agreement with literature results. However, uncertainties in estimated parameters are quite large, as expected from the results of the theoretical analysis.

Acknowledgements. P.G.P.M. and S.D. acknowledge INFN (Iniziativa specifica TAsP).

References

Appourchaux, T., Michel, E., Auvergne, M., et al. 2008, A&A, 488, 705
Asplund, M., Grevesse, N., Sauval, A. J., & Scott, P. 2009, ARA&A, 47, 481
Baglin, A., Auvergne, M., Barge, P., et al. 2009, in IAU Symposium, Vol. 253, IAU Symposium, ed. F. Pont, D. Sasselov, & M. J. Holman, 71–81
Bahcall, J. N., Pinsonneault, M. H., & Basu, S. 2001, ApJ, 555, 990
Bailin, J. 2019, ApJS, 245, 5
Basu, S., Chaplin, W. J., & Elsworth, Y. 2010, ApJ, 710, 1596
Basu, S., Verner, G. A., Chaplin, W. J., & Elsworth, Y. 2012, ApJ, 746, 76
Bonaca, A., Tanner, J. D., Basu, S., et al. 2012, ApJ, 755, L12
Borucki, W. J., Koch, D., Basri, G., et al. 2010, Science, 327, 977
Brown, T. M., Gilliland, R. L., Noyes, R. W., & Ramsey, L. W. 1991, ApJ, 368, 599
Caputo, F. et al. 1985, aap, 143, 8
Casagrande, L., Silva Aguirre, V., Stello, D., et al. 2014, ApJ, 787, 110
Chaboyer, B., Fenton, W. H., Nelan, J. E., Patnaude, D. J., & Simon, F. E. 2001, ApJ, 562, 521
Chaplin, W. J., Basu, S., Huber, D., et al. 2014, ApJS, 210, 1
Clausen, J. V., Bruntt, H., Claret, A., et al. 2009, A&A, 502, 253
Das, P., Hawkins, K., & Jofré, P. 2020, MNRAS, 493, 5195
Degl'Innocenti, S., Prada Moroni, P. G., Marconi, M., & Ruoppo, A. 2008, Ap&SS, 316, 25
Deheuvels, S. & Michel, E. 2011, A&A, 535, A91
Dell'Omodarme, M. & Valle, G. 2013, The R Journal, 5, 108
Dell'Omodarme, M., Valle, G., Degl'Innocenti, S., & Prada Moroni, P. G. 2012, A&A, 540, A26
Dotter, A., Sarajedini, A., Anderson, J., et al. 2010a, ApJ, 708, 698
Dotter, A. et al. 2010b, apj, 708, 698
Epstein, C. R., Elsworth, Y. P., Johnson, J. A., et al. 2014, ApJ, 785, L28
Gai, N., Basu, S., Chaplin, W. J., & Elsworth, Y. 2011, ApJ, 730, 63
Gaulme, P., McKeever, J., Jackiewicz, J., et al. 2016, ApJ, 832, 121
Gilliland, R. L., Brown, T. M., Christensen-Dalsgaard, J., et al. 2010, PASP, 122, 131
Gratton, R. G., Johnson, C. I., Lucatello, S., D'Orazi, V., & Pilachowski, C. 2011, A&A, 534, A72
Grunblatt, S. K., Zinn, J. C., Price-Whelan, A. M., et al. 2021, ApJ, 916, 88
Gruyters, P., Nordlander, T., & Korn, A. J. 2014, A&A, 567, A72
Guo, J.-C., Liu, C., & Liu, J.-F. 2016, Research in Astronomy and Astrophysics, 16, 44
Hansen, B. M. S. et al. 2002, apjl, 574, L155
Hendricks, B., Stetson, P. B., VandenBerg, D. A., & Dall'Ora, M. 2012, AJ, 144, 25
Jofré, P. & Weiss, A. 2011, A&A, 533, A59
Jørgensen, B. R. & Lindegren, L. 2005, A&A, 436, 127
Kjeldsen, H. & Bedding, T. R. 1995, A&A, 293, 87
Korn, A. J., Grundahl, F., Richard, O., et al. 2007, ApJ, 671, 402
Kroupa, P. 2002, Science, 295, 82
Lebreton, Y., Goupil, M. J., & Montalbán, J. 2014, in EAS Publications Series, Vol. 65, EAS Publications Series, 99–176
Magic, Z., Weiss, A., & Asplund, M. 2015, A&A, 573, A89
Malavolta, L., Sneden, C., Piotto, G., et al. 2014, AJ, 147, 25
Marino, A. F., Villanova, S., Piotto, G., et al. 2008, A&A, 490, 625
Mathur, S., Metcalfe, T. S., Woitaszek, M., et al. 2012, ApJ, 749, 152
Matsuno, T., Aoki, W., Casagrande, L., et al. 2021, ApJ, 912, 72
Michel, E., Baglin, A., Auvergne, M., et al. 2008, Science, 322, 558
Miglio, A., Chaplin, W. J., Brogaard, K., et al. 2016, MNRAS, 461, 760
Miglio, A., Girardi, L., Grundahl, F., et al. 2021, Experimental Astronomy, 51, 963
Montalbán, J., Mackereth, J. T., Miglio, A., et al. 2021, Nature Astronomy, 5, 640
Mucciarelli, A. & Bellazzini, M. 2020, Research Notes of the American Astronomical Society, 4, 52
Nordlander, T., Korn, A. J., Richard, O., & Lind, K. 2012, ApJ, 753, 48
Planck Collaboration, Aghanim, N., Akrami, Y., et al. 2020, A&A, 641, A6
Ramírez, I. & Meléndez, J. 2005, ApJ, 626, 465
Ricker, G. R., Winn, J. N., Vanderspek, R., et al. 2015, Journal of Astronomical Telescopes, Instruments, and Systems, 1, 014003
Riello, M., De Angeli, F., Evans, D. W., et al. 2020, arXiv e-prints, arXiv:2012.01916
Rodrigues, T. S., Bossini, D., Miglio, A., et al. 2017, MNRAS, 467, 1433
Salaris, M. & Weiss, A. 2002a, aap, 388, 492
Salaris, M. & Weiss, A. 2002b, A&A, 388, 492
Salpeter, E. E. 1955, ApJ, 121, 161
Sanders, J. L. & Das, P. 2018, MNRAS, 481, 4093
Sandquist, E. L., Jessen-Hansen, J., Shetrone, M. D., et al. 2016, ApJ, 831, 11
Sharma, S., Stello, D., Bland-Hawthorn, J., Huber, D., & Bedding, T. R. 2016, ApJ, 822, 15
Silva Aguirre, V., Lund, M. N., Antia, H. M., et al. 2017, ApJ, 835, 173
Soderblom, D. R. 2010, ARA&A, 48, 581
Stello, D., Saunders, N., Grunblatt, S., et al. 2022, MNRAS, 512, 1677
Stetson, P. B., Pancino, E., Zocchi, A., Sanna, N., & Monelli, M. 2019, MNRAS, 485, 3042
Tailo, M., Corsaro, E., Miglio, A., et al. 2022, A&A, 662, L7
Takeda, G., Ford, E. B., Sills, A., et al. 2007, ApJS, 168, 297
Tanner, J. D., Basu, S., & Demarque, P. 2014, ApJ, 785, L13
Tayar, J., Claytor, Z. R., Huber, D., & van Saders, J. 2022, ApJ, 927, 31
Thoul, A. A., Bahcall, J. N., & Loeb, A. 1994, ApJ, 421, 828
Tognelli, E., Dell'Omodarme, M., Valle, G., Prada Moroni, P. G., & Degl'Innocenti, S. 2021, MNRAS, 501, 383
Trampedach, R. & Stein, R. F. 2011, ApJ, 731, 78
Ulrich, R. K. 1986, ApJ, 306, L37
Valle, G., Dell'Omodarme, M., Prada Moroni, P. G., & Degl'Innocenti, S. 2014, A&A, 561, A125
Valle, G., Dell'Omodarme, M., Prada Moroni, P. G., & Degl'Innocenti, S. 2015a, A&A, 579, A59
Valle, G., Dell'Omodarme, M., Prada Moroni, P. G., & Degl'Innocenti, S. 2015b, A&A, 577, A72
Valle, G., Dell'Omodarme, M., Prada Moroni, P. G., & Degl'Innocenti, S. 2015c, A&A, 575, A12
Valle, G., Dell'Omodarme, M., Prada Moroni, P. G., & Degl'Innocenti, S. 2018a, A&A, 620, A168
Valle, G., Dell'Omodarme, M., Prada Moroni, P. G., & Degl'Innocenti, S. 2020, A&A, 635, A77
Valle, G., Dell'Omodarme, M., Tognelli, E., Prada Moroni, P. G., & Degl'Innocenti, S. 2018b, A&A, 619, A158
Valle, G., Marconi, M., Degl'Innocenti, S., & Prada Moroni, P. G. 2009, A&A, 507, 1541
VandenBerg, D. A., Brogaard, K., Leaman, R., & Casagrande, L. 2013a, ApJ, 775, 134
VandenBerg, D. A. et al. 2013b, apj, 775, 134
Viani, L. S., Basu, S., Chaplin, W. J., Davies, G. R., & Elsworth, Y. 2017, ApJ, 843, 11
Wagner-Kaiser, R. et al. 2017, mnras, 468, 1038
White, T. R., Bedding, T. R., Stello, D., et al. 2011, ApJ, 743, 161
Yıldız, M. 2007, MNRAS, 374, 1264
Yu, J., Huber, D., Bedding, T. R., et al. 2018, ApJS, 236, 42

Appendix A: Tables

Table A.1. SCEPtER median (q_{50}) and 1σ envelope boundaries (q_{16} and q_{84}) for age relative error as a function of the mass of the star in MS. Values are expressed as percent.

Main Sequence									
	Mass ($M_\odot$)								
	0.70	0.72	0.74	0.76	0.78	0.80	0.82	0.84	0.86
	C1								
q_{16}	-22.5	-23.0	-20.8	-18.8	-17.2	-16.4	-16.8	-17.2	-17.3
q_{50}	-3.8	-1.7	-0.3	0.3	0.0	0.0	0.1	0.2	0.5
q_{84}	8.6	14.9	19.2	21.6	21.4	20.7	21.2	22.5	24.2
	C2								
q_{16}	-22.5	-20.8	-19.2	-17.6	-16.1	-15.4	-16.0	-16.8	-17.6
q_{50}	-2.5	-1.2	-0.3	0.1	0.1	0.1	-0.2	-0.6	-1.3
q_{84}	6.4	12.9	17.4	19.9	19.4	18.6	19.0	19.7	20.6
	C3								
q_{16}	-32.6	-30.5	-28.2	-25.9	-23.7	-22.7	-24.0	-25.3	-25.9
q_{50}	-4.3	-2.3	-0.9	-0.0	0.2	0.1	-0.6	-1.6	-2.5
q_{84}	6.1	14.2	20.7	25.8	27.8	28.1	28.7	29.8	31.1
	$\alpha_{\rm ml}$ = 1.74								
q_{16}	-11.9	-11.1	-10.3	-9.5	-8.6	-7.9	-8.1	-8.7	-9.5
q_{50}	2.6	5.8	7.7	8.4	7.7	7.9	8.6	9.6	11.1
q_{84}	12.1	19.4	24.9	28.7	29.5	29.0	29.0	29.6	30.7
	no diffusion								
q_{16}	-60.9	-57.0	-53.5	-50.3	-47.8	-45.8	-43.6	-39.9	-34.4
q_{50}	-41.4	-39.0	-36.9	-35.2	-34.0	-32.8	-30.5	-26.2	-20.0
q_{84}	-20.9	-19.7	-18.7	-17.9	-17.3	-16.2	-13.7	-9.4	-3.7

Notes. Typical Monte Carlo relative uncertainty on q_{16} and q_{84} is about 5%, while the absolute uncertainty on q_{50} is about 0.5%.

Table A.2. Same as Tab. A.1 but for SGB stars.

Sub-Giant Branch										
	Mass ($M_\odot$)									
	0.74	0.76	0.78	0.80	0.82	0.84	0.86	0.88	0.90	0.92
	C1									
q_{16}	-13.2	-13.0	-12.9	-12.7	-13.0	-13.7	-14.4	-14.2	-13.3	-11.8
q_{50}	0	-0.1	-0.1	-0.1	0	0.1	0.4	0.9	1.4	1.8
q_{84}	15.8	15.4	15.3	15.3	16.0	17.7	19.8	20.8	21.1	20.6
	C2									
q_{16}	-12.9	-12.5	-12.2	-12.0	-12.0	-12.6	-13.4	-13.3	-12.6	-11.2
q_{50}	0.0	-0.0	-0.0	-0.0	-0.0	-0.0	0.1	0.5	0.9	1.3
q_{84}	15.5	15.0	14.7	14.5	14.9	15.9	17.3	17.9	17.9	17.2
	C3									
q_{16}	-17.4	-17.5	-17.5	-17.3	-17.4	-18.2	-19.3	-18.3	-16.0	-12.1
q_{50}	0.1	0.0	0.0	0.0	0.0	-0.0	-0.1	-0.1	0.1	0.4
q_{84}	19.4	20.9	22.2	23.2	24.1	24.8	25.2	24.7	23.5	21.6
	$\alpha_{\rm ml}$ = 1.74									
q_{16}	-8.7	-8.5	-8.2	-8.1	-8.0	-8.5	-9.3	-9.5	-9.1	-8.1
q_{50}	4.9	4.8	4.7	4.6	4.5	4.6	4.9	5.2	5.2	4.9
q_{84}	21.3	20.8	20.5	20.4	20.9	22.1	23.7	24.0	23.1	21.0
	no diffusion									
q_{16}		-38.8	-37.9	-36.8	-35.4	-32.8	-28.3	-23.1	-17.7	-12.2
q_{50}		-29.0	-28.2	-26.9	-24.8	-20.9	-15.2	-9.7	-4.3	0.9
q_{84}		-14.9	-13.6	-11.9	-9.3	-4.9	0.9	6.3	11.3	15.9

Table A.3. Same as Tab. A.1 but for RGB stars.

Red Giant Branch										
	Mass ($M_\odot$)									
	0.76	0.78	0.80	0.82	0.84	0.86	0.88	0.90	0.92	0.94
	C1									
q_{16}	-39.4	-40.0	-40.1	-39.5	-38.2	-35.8	-32.5	-29.2	-25.8	-22.4
q_{50}	1.8	1.4	1.1	1.0	1.2	1.5	1.7	1.6	1.5	1.3
q_{84}	37.1	44.0	51.4	59.6	67.1	72.1	74.3	75.6	76.2	76.2
	C2									
q_{16}	-19.6	-19.3	-19.3	-19.3	-19.5	-19.9	-20.2	-20.1	-19.5	-18.5
q_{50}	0.0	0.0	0.0	0.0	0.0	-0.0	-0.0	0.0	0.0	0.1
q_{84}	25.5	25.1	24.8	24.6	24.7	25.2	25.9	26.3	26.6	26.7
	C3									
q_{16}	-34.6	-35.1	-35.2	-35.1	-34.7	-33.3	-31.0	-28.2	-25.0	-21.4
q_{50}	0.3	0.4	0.5	0.4	0.4	0.2	0.1	0.4	1.4	3.0
q_{84}	35.7	41.6	47.1	52.7	56.9	59.2	60.1	60.6	61.5	62.7
	$\alpha_{\rm ml}$ = 1.74									
q_{16}	-21.9	-21.9	-21.9	-21.8	-22.1	-22.6	-23.0	-22.8	-22.0	-20.6
q_{50}	-2.0	-2.3	-2.7	-3.2	-3.6	-3.8	-3.8	-3.8	-3.8	-3.7
q_{84}	20.7	20.4	20.4	20.7	21.3	22.1	22.7	22.8	22.4	21.6
	no diffusion									
q_{16}		-22.5	-22.2	-22.0	-21.9	-22.2	-22.5	-22.6	-22.5	-22.2
q_{50}		-3.6	-3.4	-3.2	-3.1	-3.0	-2.9	-2.9	-3.0	-3.3
q_{84}		20.9	20.8	20.9	21.2	21.6	22.1	22.6	22.5	21.7

Table A.4. SCEPtER median (q_{50}) and 1σ envelope boundaries (q_{16} and q_{84}) for age relative error as a function of the relative age of the star during the MS. Notice that MS relative age lower than 0.4 do not enter in our sample as they're simply too young.

Main Sequence							
	relative age						
	0.4	0.5	0.6	0.7	0.8	0.9	1.0
	C1						
q_{16}	-29.7	-28.1	-25.6	-22.6	-19.7	-17.2	-15.4
q_{50}	-5.9	-4.3	-2.8	-1.6	-0.7	-0.2	0.0
q_{84}	9.6	11.4	13.3	15.6	17.4	18.3	18.5
	C2						
q_{16}	-25.4	-24.4	-22.7	-20.5	-18.3	-16.2	-14.4
q_{50}	-3.6	-2.8	-1.9	-1.0	-0.3	0.0	-0.0
q_{84}	4.1	7.6	11.0	14.1	16.2	17.0	16.8
	C3						
q_{16}	-34.5	-34.1	-32.9	-30.8	-27.9	-24.4	-21.0
q_{50}	-5.7	-4.4	-3.2	-2.1	-1.1	-0.4	0.0
q_{84}	5.0	8.1	12.0	16.3	19.4	21.9	23.5
	$\alpha_{\rm ml}$ = 1.74						
q_{16}	-12.1	-12.4	-12.1	-11.2	-10.1	-9.2	-8.4
q_{50}	4.2	3.7	3.8	4.8	6.5	7.1	6.5
q_{84}	12.5	15.3	18.2	21.4	23.9	24.9	24.5
	no diffusion						
q_{16}	-66.7	-62.5	-57.9	-53.6	-50.2	-46.5	-42.9
q_{50}	-45.6	-42.9	-39.8	-37.1	-35.1	-33.1	-31.2
q_{84}	-23.1	-20.7	-19.0	-18.4	-18.0	-16.9	-15.5

Table A.5. Same as Tab. A.4 but for SGB stars.

Sub-Giant Branch										
	relative age									
	0.1	0.2	0.3	0.4	0.5	0.6	0.7	0.8	0.9	1.0
	C1									
q_{16}	-13.2	-12.9	-12.6	-12.4	-12.3	-12.2	-12.4	-13.3	-14.7	-16.8
q_{50}	-0	0.1	0.1	0.1	0.1	0	-0.1	-0.2	-0.3	-0.5
q_{84}	15.9	15.6	15.3	15.0	14.9	14.8	15.1	16.7	19.9	24.8
	C2									
q_{16}	-12.7	-12.4	-12.2	-12.0	-11.8	-11.7	-11.8	-12.4	-13.3	-14.7
q_{50}	0	0	0	0	0	0	-0	-0	0	0
q_{84}	15.5	15.2	15.0	14.8	14.7	14.4	14.5	15.2	16.7	19.1
	C3									
q_{16}	-18.2	-17.5	-17.0	-16.6	-16.3	-16.0	-16.3	-17.3	-19.0	-21.5
q_{50}	0	0.1	0.1	0	0	0	0	-0	-0.1	-0.3
q_{84}	22.2	21.9	21.6	21.4	21.1	20.4	20.3	22.1	26.1	32.5
	$\alpha_{\rm ml}$ = 1.74									
q_{16}	-8.0	-7.9	-7.9	-7.9	-8.0	-7.9	-8.1	-8.8	-9.9	-11.5
q_{50}	5.3	5.2	5.1	4.9	4.8	4.7	4.3	3.9	3.6	3.4
q_{84}	22.1	21.7	21.3	20.8	20.4	20.0	19.8	20.2	21.3	23.2
	no diffusion									
q_{16}	-40.4	-39.8	-39.1	-38.3	-37.4	-36.2	-34.2	-31.4	-27.8	-23.3
q_{50}	-29.9	-29.6	-29.1	-28.5	-27.7	-26.6	-24.4	-20.8	-16.1	-10.1
q_{84}	-16.2	-15.9	-15.6	-15.1	-14.3	-13.0	-10.4	-6.3	-0.6	6.7

Table A.6. Same as Tab. A.4 but for RGB stars.

Red Giant Branch										
	relative age									
	0.1	0.2	0.3	0.4	0.5	0.6	0.7	0.8	0.9	1.0
	C1									
q_{16}	-29.4	-33.8	-37.2	-39.7	-40.6	-40.6	-40.2	-39.5	-38.6	-37.4
q_{50}	2.2	2.1	1.6	1.0	0.6	0.2	0	0.2	1.0	2.2
q_{84}	48.0	51.2	53.6	55.2	56.1	56.7	57.1	57.3	57.0	56.2
	C2									
q_{16}	-19.2	-19.7	-20.1	-20.3	-20.2	-20.1	-19.8	-19.4	-18.7	-17.8
q_{50}	0.1	0.1	0.1	0.0	-0.0	-0.0	-0.0	-0.0	-0.0	0.0
q_{84}	25.9	25.8	25.5	25.0	24.6	24.6	24.6	24.5	24.3	24.1
	C3									
q_{16}	-31.0	-33.3	-34.8	-35.7	-35.8	-35.4	-34.8	-33.8	-32.5	-30.7
q_{50}	2.5	2.1	1.5	0.6	0	-0	0	0	0	0
q_{84}	47.7	48.7	49.1	48.8	48.1	47.2	46.8	46.6	46.4	46.2
	$\alpha_{\rm ml}$ = 1.74									
q_{16}	-17.9	-20.0	-21.6	-22.6	-23.0	-23.1	-23.3	-23.5	-23.8	-24.0
q_{50}	1.0	-0.6	-2.0	-3.2	-4.0	-4.4	-4.9	-5.1	-5.0	-4.3
q_{84}	25.1	23.7	22.2	20.7	19.7	19.2	18.8	18.8	19.4	20.6
	no diffusion									
q_{16}	-24.2	-23.2	-22.3	-21.9	-21.4	-21.3	-21.6	-21.6	-21.5	-21.2
q_{50}	-4.5	-3.4	-2.9	-2.7	-2.8	-3.0	-3.1	-3.1	-3.0	-2.9
q_{84}	20.5	21.8	22.2	21.9	21.2	20.8	20.8	21.1	21.6	22.2